This document is downloaded from DR-NTU (https://dr.ntu.edu.sg)
Nanyang Technological University, Singapore.

Temporal wavelet analysis for deformation and velocity measurement in speckle interferometry

Fu, Yu; Tay, Cho Jui; Quan, Chenggen; Chen, Lujie

2004

Fu, Y., Tay, C. J., Quan, C., & Chen, L. (2004). Temporal wavelet analysis for deformation and velocity measurement in speckle interferometry. Optical Engineering, 43(11), 2780-2787.

https://hdl.handle.net/10356/91918

https://doi.org/10.1117/1.1801472

Copyright 2004 Society of Photo-Optical Instrumentation Engineers. One print or electronic copy may be made for personal use only. Systematic reproduction and distribution, duplication of any material in this paper for a fee or for commercial purposes, or modification of the content of the paper are prohibited.

Downloaded on 23 Aug 2022 16:02:30 SGT

Temporal wavelet analysis for deformation and velocity measurement in speckle interferometry

Y. Fu
C. J. Tay
C. Quan
L. J. Chen
National University of Singapore
Department of Mechanical Engineering
10 Kent Ridge Crescent
Singapore 119260

Abstract. When a continuously deforming object is measured by electronic speckle pattern interferometry (ESPI), the speckle pattern recorded on a camera sensor changes constantly. These time-dependent speckle patterns would provide the deformation history of the object. Various objects are applied with both linearly and nonlinearly varying loads and speckle patterns are captured using a high-speed CCD camera. The temporal intensity variation of each pixel on the recorded images is analyzed by a robust mathematical tool—Morlet wavelet transform instead of conventional Fourier transform. The transient velocity and displacement of each point can be retrieved without the necessity of the temporal or spatial phase unwrapping process. The displacements obtained are compared with those from a temporal Fourier transform, and the results show that the wavelet transform minimizes the influence of noise and provides better results for a linearly varying load. System error in the wavelet analysis for nonlinear load is also discussed. © *2004 Society of Photo-Optical Instrumentation Engineers.* [DOI: 10.1117/1.1801472]

Subject terms: high-speed imaging; continuous wavelet transforms; temporal phase analysis; speckle interferometry; instantaneous frequency.

Paper 030642 received Dec. 24, 2003; revised manuscript received Apr. 22, 2004; accepted for publication May 5, 2004.

1 Introduction

Electronic speckle pattern interferometry (ESPI) is one of the most commonly used methods for high-resolution measurements. It is a nondestructive, whole-field technique for static and dynamic deformation measurements. A phase-shifting technique is usually applied with ESPI to retrieve accurate phase values from speckle patterns. However, it requires several, normally three to five images, together with prescribed phase steps. For this reason, phase-shifting approaches are not easily accomplished in continuous deformation measurement.[1]

Temporal phase analysis and temporal phase unwrapping techniques[2–4] were introduced to overcome this problem in the late 1990s. Early applications involve contouring surface with discontinuities by wavelength-scanning interferometry.[5,6] Joenathan et al.[7–9] developed a novel approach based on temporal speckle pattern interferometry (TSPI) to measure large continuous deformation of objects. While an object deforms, the phase of speckles on an image sensor would fluctuate and a high-speed CCD camera is usually arranged to record the speckle patterns. Each pixel is then analyzed as a function of time. The phase of the speckles is related to the in-plane or out-of-plane displacement or the slope of the deformation, depending on the optical arrangements. The reported upper limit on the object deformation measurement using the temporal analysis technique is more than 100 μm instead of 6 to 7 μm, as in conventional spatial techniques.

Although some phase analysis algorithms[10] have been introduced, the Fourier transform[11] is still a predominant method in temporal phase analysis. The intensity fluctuation due to deformation of each pixel is first transformed, and one side of the spectrum is filtered with a bandpass filter. The filtered spectrum is inverse-transformed to obtain the wrapped phase. The phase values are then unwrapped along the time axis at each pixel independently of other pixels in the image. It is well known that the accuracy of the Fourier transform analysis increases for higher temporal frequency with a narrow spectrum. In most cases, however, the deformation of each point on the object is different, and the deformation of each pixel may also be nonlinear along the time axis. An automatic filtering process becomes difficult as the width of the bandpass filter must be broadened, and introduces further errors in phase extraction.

The shortcoming of the mentioned Fourier analysis can be overcome by using a wavelet transform. The wavelet transform[12] is a relatively new and robust mathematical tool for signal analysis. Recently, it has also gained popularity in optical interferometry and has been applied successfully to denoise speckle patterns.[13–15] Continuous wavelet transforms (CWTs) were also used for phase extraction on different types of open-fringe interferograms or fringe patterns with spatial carriers.[16–18] These applications use 1-D CWTs along one spatial axis. The phase gradient can be obtained by extracting the "ridge" of the wavelet coefficients, followed by an integration process to retrieve the phase. A wavelet transform has also been applied on temporal phase analysis of speckle interferometry. The concept was first introduced by Colonna de Lega in 1996 and some preliminary results were presented.[19,20] Cherbuliez

 © 2004 Society of Photo-Optical Instrumentation Engineers

Downloaded from SPIE Digital Library on 25 Aug 2010 to 155.69.4.4. Terms of Use: http://spiedl.org/terms

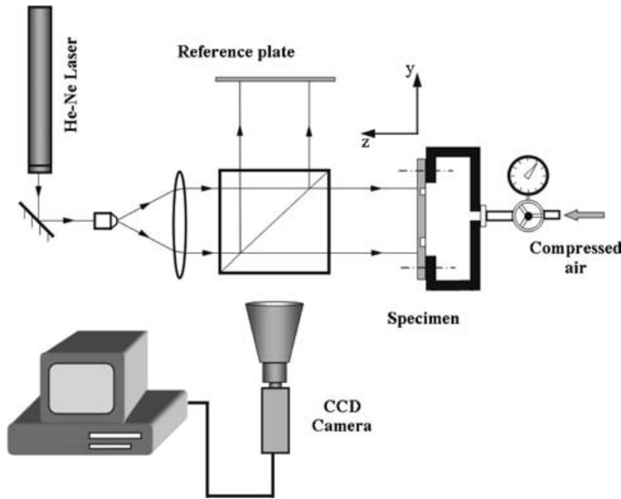

Fig. 1 Schematic layout of ESPI system.

et al.,[21] Cherbuliez and Jacquot,[22] and Cherbuliez[23] extended the study on applying different processing algorithms to develop a fast and efficient software tool for phase retrieval from dynamic fringe or speckle patterns.

In this paper, a complex Morlet wavelet function is used to extract instantaneous frequency at each pixel from a series of speckle patterns obtained by ESPI. The instantaneous velocity, which is useful in dynamic measurement, is derived directly from the frequency. Unlike Colonna de Lega's method, out-of-plane displacement is retrieved by integration and a phase-unwrapping process in time and its spatial domain is not required. Displacement obtained using temporal wavelet analysis is also compared with that using conventional temporal Fourier analysis.

2 Theoretical Analysis

A schematic layout of ESPI setup for out-of-plane measurement is shown in Fig. 1. An expanded laser beam is collimated and separated by a beamsplitter into object and reference beams. A series of speckle patterns are captured by a high-speed CCD camera with a telecentric lens during deformation. The intensity of each pixel can be expressed as

$$I_{xy}(t)=I_{0_{xy}}(t)+A_{xy}(t)\cos[\varphi_{xy}(t)]$$
$$=I_{0_{xy}}(t)\left\{1+V\cos\left[\phi_{0_{xy}}+\frac{4\pi z_{xy}(t)}{\lambda}\right]\right\}, \quad (1)$$

where $I_{0_{xy}}(t)$ is the intensity bias of the speckle pattern, V is the visibility, $\phi_{0_{xy}}$ is a random phase, and $z_{xy}(t)$ is the out-of-plane deformation of the object. A series of speckle patterns are recorded during the deformation and at each pixel, the intensity variation is analyzed by CWT.

The CWT $W_S(a,b)$ maps a function $s(t)$ onto a 2-D domain (time-scale plane). It can be expressed by

$$W_S(a,b)=\int_{-\infty}^{+\infty}s(t)h_{ab}^{*}(t)\mathrm{d}t, \quad (2)$$

where

$$h_{ab}(t)=\frac{1}{\sqrt{a}}h\left(\frac{t-b}{a}\right), \quad (3)$$

$h(t)$ is known as the mother wavelet; $h_{ab}(t)$ are the basis functions of the transform, known as daughter wavelets; $a\neq 0$ is a dilation scale parameter related to the frequency; b is a position parameter along the time axis; and * denotes the complex conjugate. The factor $1/\sqrt{a}$ in Eq. (3) is used to keep the energy of $h_{ab}(t)$ constant during dilation and translation.

The signal $s(t)$ can be recovered from the wavelet coefficients $W_S(a,b)$ by an inverse wavelet transform given by[12]:

$$s(t)=\frac{1}{C}\int_{-\infty}^{+\infty}\int_{-\infty}^{+\infty}W_S(a,b)h\left(\frac{t-b}{a}\right)\frac{\mathrm{d}a}{a^2}\mathrm{d}b, \quad (4)$$

where the constant C depends only on $h(t)$ and is given by

$$C=2\pi\int_{-\infty}^{+\infty}\frac{|\hat{h}(\omega)|^2}{|\omega|}\mathrm{d}\omega<\infty, \quad (5)$$

where $\hat{h}(\omega)$ denotes the Fourier transform of $h(t)$. The requirement that constant C has to be less than infinity leads to the so-called admissibility condition on the mother wavelet functions. If $h(t)$ is[1] in $\mathbf{L}(R)$, then $\hat{h}(\omega)$ is continuous, hence C can be finite only if $\hat{h}(0)=0$, which implies that the mother wavelet function $h(t)$ has an average of zero value.

In this paper, the velocity and displacement, which are derived from the instantaneous frequencies of intensity variation, are measured using wavelets. An analytic wavelet is selected as the amplitude and phase of the signal are to be separated. A particular choice for the mother wavelet is the Morlet wavelet, which is widely used in the study of signals with strong components of pure sinusoidal or modulated sinusoidal waves. The Morlet wavelet has the form

$$h(t)=g(t)\exp(i\omega_0 t), \quad (6)$$

where $g(t)=\exp(-t^2/2)$, and ω_0 is the "mother" frequency, the only parameter that must be chosen. One consideration is that $\hat{h}(0)$ is numerically negligible. This condition is verified when $\omega_0>5$. Interference effects introduced by the Morlet wavelet must also be considered when ω_0 is selected.[20] Here $\omega_0=2\pi$ is chosen to satisfy the admissibility condition so that the wavelet function is able to remove the negative frequencies as well as avoid the dc contribution of the signals.[24]

In a CWT, a kernel that consists of a scaled template waveform shifts along the signal and calculates the wavelet coefficient that represents how closely correlated the wavelet is with this section of the signal. In this paper, it expands a 1-D temporal intensity variation of certain pixels to a 2-D plane of scaling a (which is related to the frequency) and position b (which is related to the time axis).

Downloaded from SPIE Digital Library on 25 Aug 2010 to 155.69.4.4. Terms of Use: http://spiedl.org/terms

To avoid a large error in the CWT at the boundary, the intensity variation signal on each pixel is extended at its left- and right-hand edges. Symmetrical or zero padding extension techniques are commonly adopted in the practice. In this paper, a linear predictive extrapolation method[25] is selected. The advantage of this extrapolation method is that phase and frequency of intensity variations are maintained. After the CWT has been carried out on the extended data, the wavelet coefficients are truncated appropriately.

Substituting Eqs. (1) and (6) into Eq. (2), the wavelet transform of temporal intensity variation can be expressed as[26]

$$W_{xy}(a,b)=\frac{\sqrt{a}}{2}A_{xy}(b)\left(\hat{g}\{a[\zeta-\varphi'_{xy}(b)]\}+\epsilon\left(b,\frac{\omega_0}{a}\right)\right)\times\{\exp[i\varphi_{xy}(b)]\}, \tag{7}$$

where $\zeta=\omega_0/a$, and ϵ is a corrective term, which will remain small if the following conditions are satisfied:

$$\frac{\omega_0^2}{|\varphi'_{xy}(b)|^2}\frac{|A''_{xy}(b)|}{|A_{xy}(b)|}\ll 1, \tag{8}$$

and

$$\omega_0^2\frac{|\varphi''_{xy}(b)|}{|\varphi'_{xy}(b)|^2}\ll 1. \tag{9}$$

The presence of φ'_{xy} in the denominator shows that A'_{xy} and φ'_{xy} are slow varying if φ'_{xy} is small but may vary much more quickly for large instantaneous frequencies. As the $\exp[-i\varphi_{xy}(b)]$ and dc terms are negligible with proper selection of ω_0, only the $\exp[i\varphi_{xy}(b)]$ term remains in Eq. (7). Delprat et al.[27] shows a different proof with similar results using a stationary phase approximation.

The trajectory of maximum $|W_{xy}(a,b)|$ on the a-b plane is called a "ridge." If $A_{xy}(b)$ and $\varphi'_{xy}(b)$ have small variations over the support of h_{ab}, and $\varphi'_{xy}(b)\geqslant\Delta\omega/a$, ϵ is negligible, and the instantaneous frequency can be obtained by

$$\varphi'_{xy}(b)=\zeta_{rb}=\frac{\omega_0}{a_{rb}}, \tag{10}$$

as $|\hat{g}(\omega)|$ has a maximum value at ω=0. Note that a_{rb} denotes the value of a at instant b on the ridge. The instantaneous velocity of point $P(x,y)$ at instant b, which is proportional to $\varphi'_{xy}(b)$, can be retrieved directly.

The wavelet transform on the ridge can then be expressed as

$$W_{xy}(a_{rb},b)\approx\frac{\sqrt{a_{rb}}}{2}A_{xy}(b)\hat{g}(0)\exp[i\varphi_{xy}(b)]. \tag{11}$$

The phase value $\varphi_{xy}(b)$, which represents the temporal displacement, can be retrieved by two methods. One method is to calculate the arctangent of the ratio of the imaginary and real parts of the wavelet transform on the ridge:

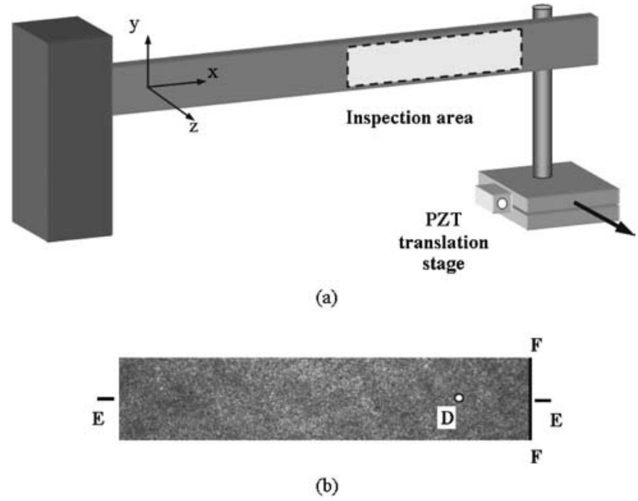

Fig. 2 (a) Cantilever beam and loading device and (b) typical speckle pattern captured by a high-speed CCD camera.

$$\varphi_{xy}(b)=\tan^{-1}\left(\frac{\mathrm{Im}[W_{xy}(a_{rb},b)]}{\mathrm{Re}[W_{xy}(a_{rb},b)]}\right) \tag{12}$$

where Re and Im denote the real and imaginary parts of the wavelet transform. However, $\varphi_{xy}(b)$ obtained from Eq. (12) is within $[0,2\pi)$ and phase unwrapping cannot be avoided. In this paper, the phase value $\varphi_{xy}(b)$ is calculated by integration of the instantaneous frequency in Eq. (10), and phase-unwrapping procedure is not required in temporal and spatial domain. Combination of phase values of each pixel at certain instant T generates a phase map of φ_T, and deformation between two instants T_1 and T_2 can be obtained by $(\varphi_{T_2}-\varphi_{T_1})$.

3 Experimental Illustration

Two test specimens are used in this study. The first specimen is a fully clamped square plate with several artificial defects (circular blind holes with different depths). The width and thickness of the plate are 80 and 5 mm, respectively. The plate is loaded by a uniformly distributed pressure applied with compressed air, and continuously deformed by increments of pressure in the chamber. The beam of a He-Ne laser (30 mW, λ=632.8 nm) illuminates the specimen and a reference plate at right angle through a beamsplitter. The object and reference beams are recorded on a CCD sensor. During deformation of the object, a series of speckle patterns is captured by a high-speed CCD camera (KODAK Motion Corder Analyzer, SR-Ultra) with a telecentric gauging lens. The second specimen is a cantilever beam, which is loaded with a nonlinear motion using a computer-controlled piezoelectrical transducer [Fig. 2(a)]. The setup is similar to the previous one. Only a portion of the beam is inspected and a typical speckle pattern is shown in Fig. 2(b).

4 Results and Discussion

Figure 3(a) shows a typical speckle pattern captured from a part of the fully clamped plate at intervals of 0.004 s with imaging rate of 250 frames/s (fps). A small area of interest

Downloaded from SPIE Digital Library on 25 Aug 2010 to 155.69.4.4. Terms of Use: http://spiedl.org/terms

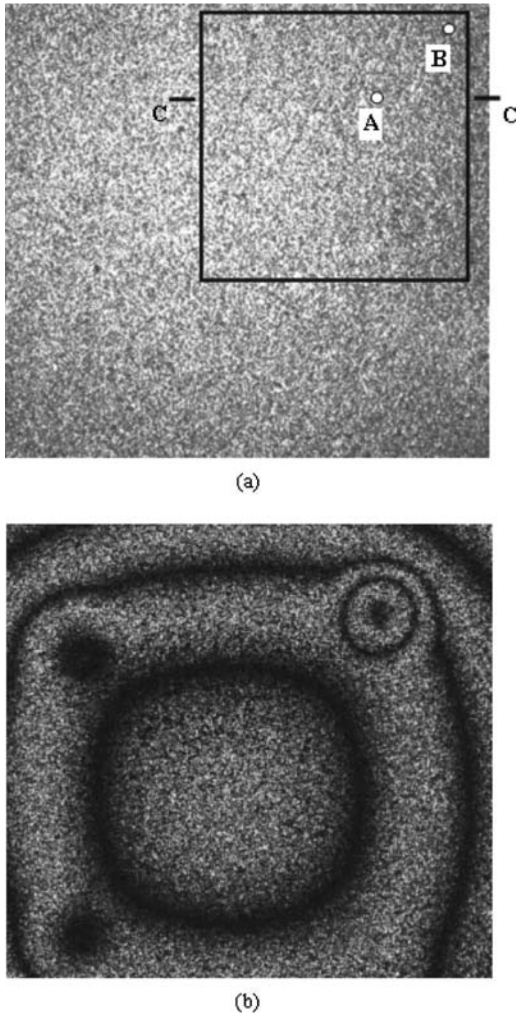

Fig. 3 (a) Area of interest on typical speckle pattern captured by a high-speed CCD camera and (b) ESPI fringes at instant $T=0.2$ s.

containing 300×300 pixels is also shown. Five hundred speckle patterns are captured during a 2-s period. Among them, 128 consecutive images are selected for processing. Figure 3(b) shows an ESPI fringe pattern at an instant $T=0.2$ s, which is obtained by subtraction of two speckle patterns. For each pixel, 128 sampling points along the time axis are obtained. Figure 4 shows the gray-value variation of points A and B [indicated in Fig. 3(a)]. A difference in

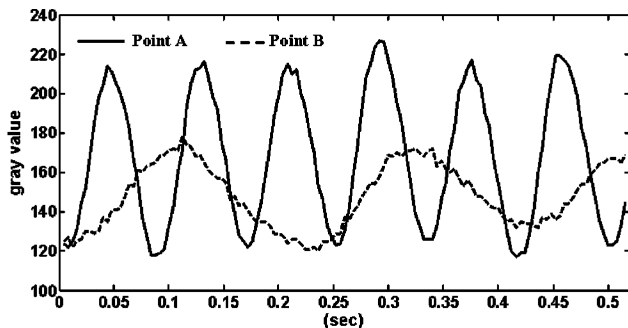

Fig. 4 Gray values of points A and B.

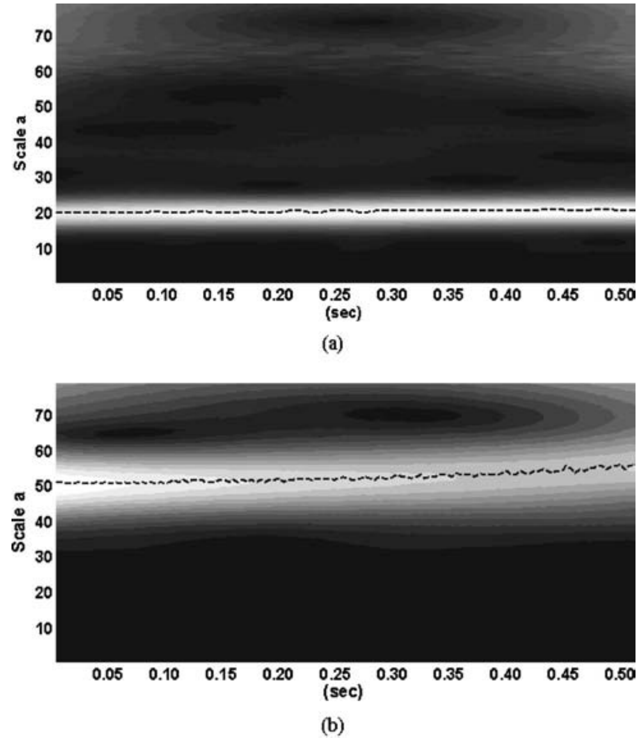

Fig. 5 Plots of the modulus of Morlet wavelet transform at (a) point A and (b) point B.

amplitude is observed due to nonuniform illumination. However, only temporal frequencies are considered as they contain information on velocity and displacement. The temporal frequency of point A is much higher than that of point B. This implies that point A deforms faster than point B. The modulus of the Morlet wavelet transform of intensity variation of points A and B are shown in Figs. 5(a) and 5(b), respectively. The dashed line shows the ridge of the wavelet transformation where the maximum moduli are found. Little variation of a_{rb} is observed on the ridge, which implies the velocities are almost constant along time axis. Figure 6(a) shows the velocities at points A and B, where the transient velocities at each pixel can be retrieved. Integration of $(2\pi)/a_{rb}$ is carried out on each pixel to generate a continuous temporal phase φ. At a certain instant T, the phase change due to the displacement can be obtained from $(\varphi_T-\varphi_{T_0})$, where φ_{T_0} is the phase at instant $T_0=0$. In an ESPI setup, as shown in Fig. 1, a 2π phase change represents a displacement of $\lambda/2$ (=316.4 nm) in the z direction. The transient displacements of points A and B are shown in Fig. 6(b). Figure 7(a) shows a 3-D plot of the out-of-plane displacement at instant $T=0.2$ s. A 3×3 median filter was used on the phase map to remove several ill-behaved pixels. The corresponding fringe pattern is shown in Fig. 3(b). Figure 7(b) shows the out-of-plane displacements on cross section C-C [indicated in Fig. 3(a)] at different instants. A smooth spatial distribution of displacement is observed.

For comparison, temporal Fourier analysis was also applied on the same speckle patterns. Bandpass filters with different widths were applied. As the temporal frequencies of each pixel are different, a relatively wider filter provides

Downloaded from SPIE Digital Library on 25 Aug 2010 to 155.69.4.4. Terms of Use: http://spiedl.org/terms

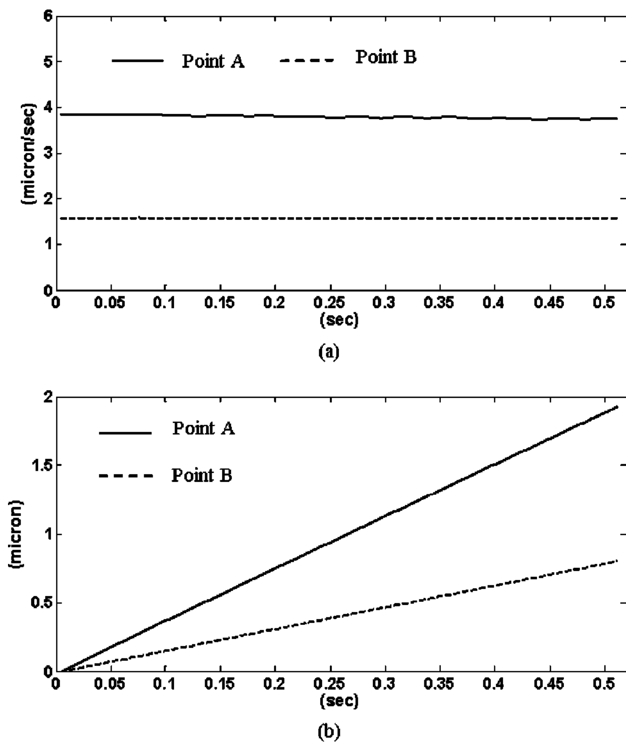

Fig. 6 Transient (a) velocities and (b) displacements of points *A* and *B*.

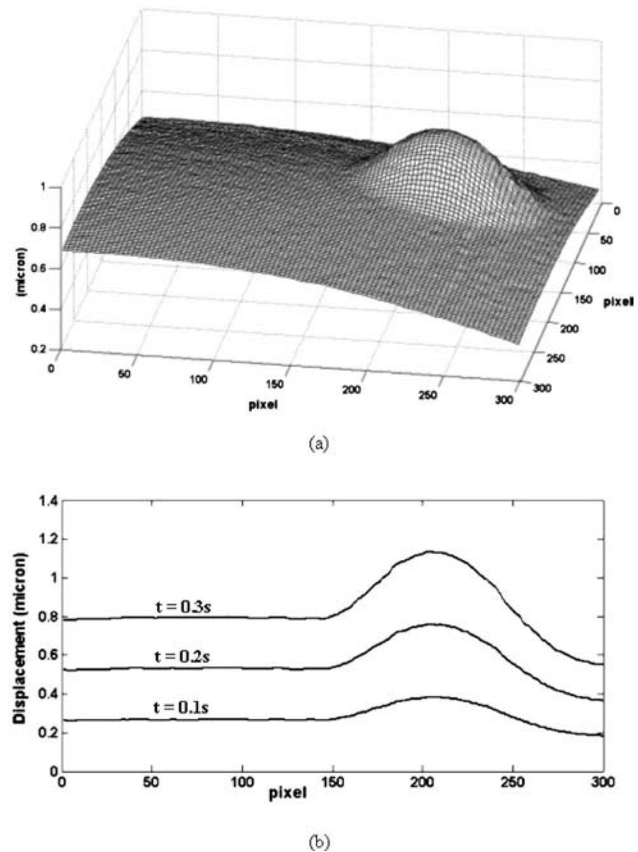

Fig. 7 (a) 3-D plot of out-of-plane displacement generated by wavelet transform and (b) transient displacements on cross section *C*-*C* obtained by wavelet transformation.

the best result as it includes all frequencies. A 1-D phase unwrapping was then applied along the time axis, as all phase values obtained by inverse Fourier transformation are within $[0,2\pi)$. Figure 8(a) shows the 3-D displacement plot from temporal Fourier analysis and Fig. 8(b) is the out-of-plane displacements at cross section *C*-*C*. As in wavelet transform, a 3×3 median filter was also applied on the phase map. However, the fluctuation due to noise is still obvious. In Figs. 7 and 8, we observe that the maximum displacement fluctuation due to noise is around 0.08 μm in the Fourier transform, but only 0.02 μm in the wavelet analysis.

In the second experiment, a slightly nonlinear loading was applied to a cantilever beam using a piezoelectrical transducer. Figure 9(a) shows modulus of the wavelet transform of intensity variation on point *D* [indicated in Fig. 2(b)]. Different values of a_{rb} on the ridge are observed, which implies the nonlinearity of the velocities. Figure 9(b) shows the velocity of point *D*, which is directly derived from instantaneous frequency in Fig. 9(a). A smooth transient displacement curve of point *D* was obtained through integration of velocity [shown in Fig. 9(c)]. Figure 10 shows the velocity distribution on cross section *E*-*E* [indicated in Fig. 2(b)] at different instants. From a comparison of the displacements using wavelet and Fourier analysis (shown in Fig. 11), we observe that CWT on each pixel generates a smoother spatial displacement distribution at different instants compared to Fourier transform. The maximum displacement fluctuation due to noise is around 0.04 μm in Fourier transform, but only 0.02 μm in wavelet analysis.

From the preceding comparison between the results of wavelet and Fourier analysis, we can observe that wavelet analysis shows better results in continuous displacement measurement. As wavelet analysis calculates the optimized frequency at each instant, it performs an adaptive bandpass filtering of the measured signal, and thus limits the influence of various noise sources and increases the resolution of measurement significantly. In contrast, the Fourier transform uses a broader filter, which is less efficient in eliminating noise effect. The maximum displacement fluctuation due to noise depends on the width of the bandpass filter and the quality of the speckle patterns.

When the loading is linearly increased, the values of $A_{xy}(b)$ and $\varphi'_{xy}(b)$ remain constant and the corrective term ϵ in Eq. (7) can be negligible. For loading that is nonlinear, a slight nonlinearity of $\varphi'_{xy}(b)$ is observed and the corrective term ϵ will affect slightly the results of the instantaneous frequency extraction. If conditions in Eq. (8) and Eq. (9) are satisfied, the errors on frequency $\varphi'_{xy}(b)$ are limited. However, when the displacement is extracted by integration, an accumulated error is observed. Compared to the Fourier transform, a slight offset can be observed in the wavelet results when the displacement is large. Comparing the averaging displacement at the right end (*F*-*F*) of the beam [shown in Fig. 2(b)], a difference of 0.04 μm is observed when the displacement is around 2.3 μm, which indicates that the system error due to ϵ is around 1.7% for

Downloaded from SPIE Digital Library on 25 Aug 2010 to 155.69.4.4. Terms of Use: http://spiedl.org/terms

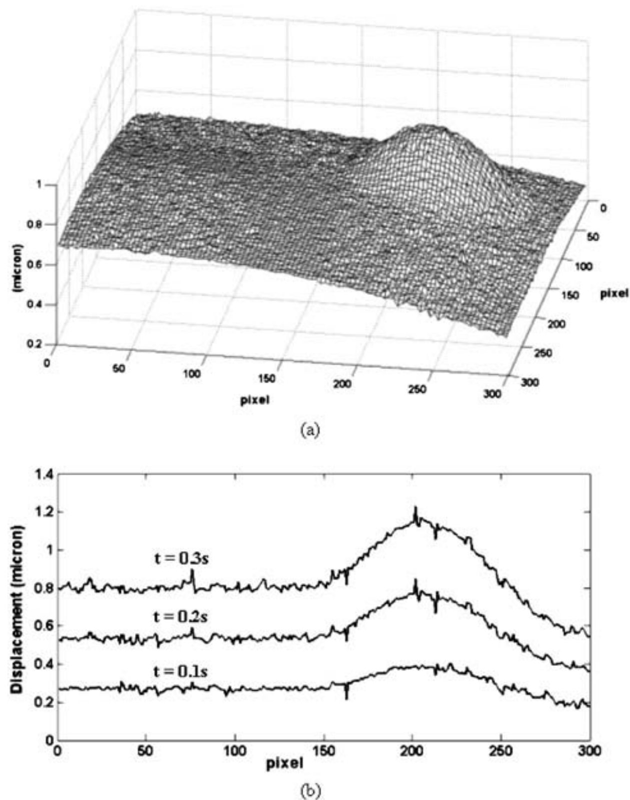

Fig. 8 (a) 3-D plot of out-of-plane displacement generated by Fourier transform and (b) transient displacements on cross section *C-C* obtained by Fourier transform.

velocities that vary between 3.7 and 4.7 μm/s [Fig. 9(b)]. Further study of the effect of ϵ with different extents of nonlinearity would be useful.

Continuous wavelet transform maps a 1-D intensity variation signal to a 2-D plane of position and frequency, and extracts the optimized frequencies. Although some fast-converging iterative algorithms[20–23] are introduced and it is not necessary to explore the whole time-frequency plane, the CWT is still a time-consuming process and requires high computing speed and memory. The computation time is about 10 times larger than that of the temporal Fourier transform. This is the main drawback of CWT in temporal phase analysis. Similar to other temporal phase analysis methods, the wavelet transform is also limited by Nyquist sampling theorem. It is impossible to analyze signals with a frequency higher than half of the acquisition rate. However, these two disadvantages have become inconspicuous due to the rapid improvement in the capacity of computers and high-speed CCD cameras.

The temporal phase analysis technique has the advantage of eliminating speckle noise, as it evaluates the phase pixel by pixel along the time axis. There are still some ill-behaved pixels, however, compared to the speckle noise in the spatial domain, these pixels can be easily identified and removed. The temporal phase analysis technique does have its disadvantages and the determination of absolute sign of the computed phase is impossible by both temporal Fourier and wavelet analysis. This limits the technique to the measurement of deformation in one direction. Furthermore, it cannot analyze a part of an object that is not mov-

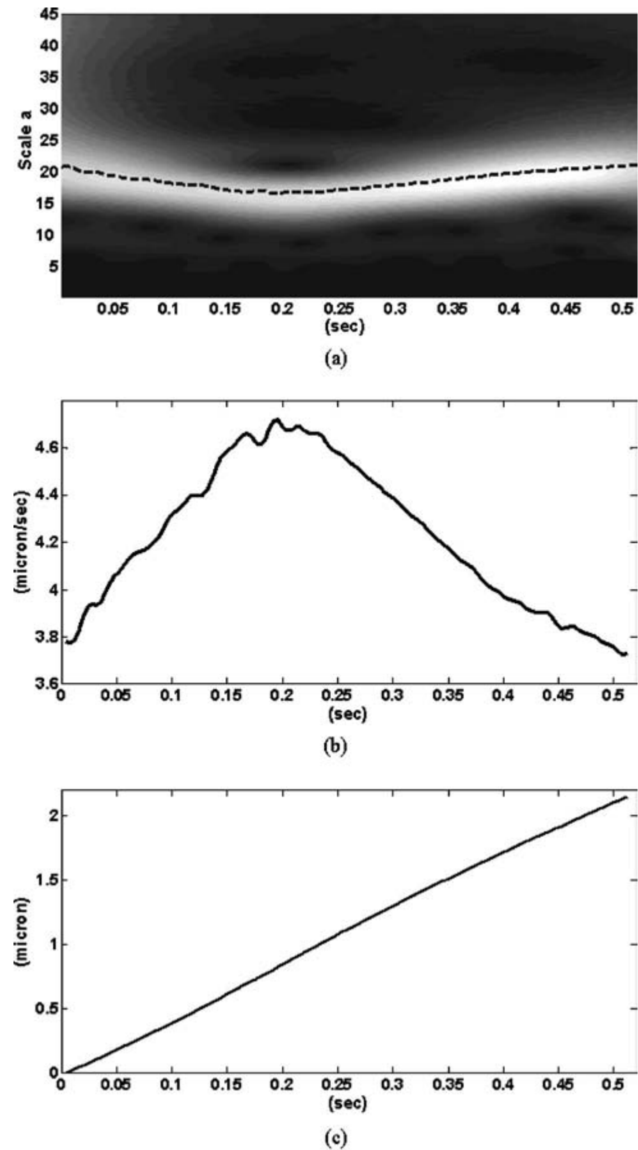

Fig. 9 (a) Plot of the modulus of Morlet wavelet transform at point *D*, (b) transient velocity of point *D*, and (c) transient displacement of point *D*.

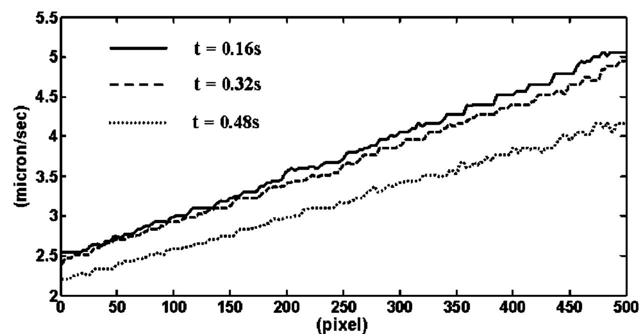

Fig. 10 Velocity distribution at cross section *E-E* at different instants.

Downloaded from SPIE Digital Library on 25 Aug 2010 to 155.69.4.4. Terms of Use: http://spiedl.org/terms

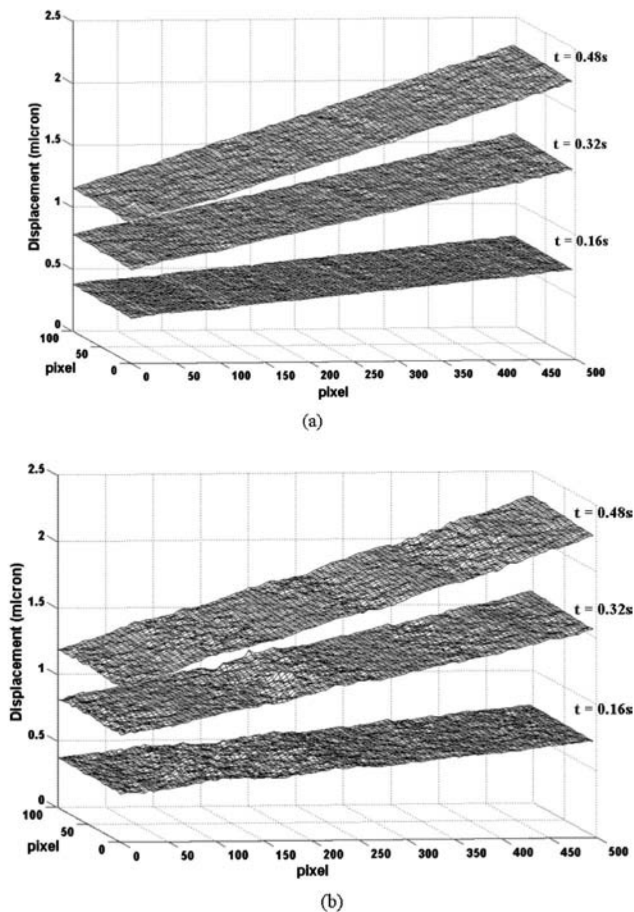

Fig. 11 Displacement of the cantilever beam at different instants obtained by (a) wavelet transform and (b) Fourier transform.

ing with the rest. Adding a carrier frequency to the image acquisition process is a method to overcome these problems.[21] However, the limitation of the mentioned Nyquist sampling theorem must be considered and sometimes a compromise is not easily reached. Another interesting point in this paper is the selection of wavelet basis functions. The complex Morlet wavelet was selected because it gives the smallest Heisenberg box. However, further study on the performance using other wavelet basis functions would also be useful.

5 Concluding Remarks

We presented a novel method to retrieve the transient velocity and displacement on a continuously deforming object using temporal wavelet analysis of speckle patterns. Unlike conventional phase evaluation techniques such as the Fourier transform, this method analyzes the phase values point by point along the time axis using a complex analytical wavelet—the Morlet wavelet transform. Compared to the Fourier transform, the wavelet has the advantages on extracting the instantaneous frequencies, from which the velocity can be retrieved directly. A high-quality deformation map of the object can also be obtained without any phase-unwrapping processes. A comparison between the temporal wavelet transform and the Fourier transform showed that wavelet analysis can limit the influence of various noise sources and significantly improve the result in displacement measurement. The maximum displacement fluctuation due to noise was limited to 0.02 μm. The system error in wavelet analysis when the loading is nonlinear was also estimated. Besides the continuous deformation and velocity measurements described in this paper, the wavelet analysis could also be applied to wavelength-scanning interferometry and other similar contouring techniques.

References

1. J. M. Huntley, G. H. Kaufmann, and D. Kerr, ''Phase-shifted dynamic speckle pattern interferometry at 1 kHz,'' *Appl. Opt.* **38**(31), 6556–6563 (1999).
2. H. J. Tiziani, ''Spectral and temporal phase evaluation for interferometry and speckle applications,'' in *Trends in Optical Nondestructive Testing and Inspection*, P. K. Rastogi and D. Inaudi, Eds., pp. 323–343, Elsevier Science B.V., **City** (2000).
3. J. M. Huntley and H. Saldner, ''Temporal phase-unwrapping algorithm for automated interferogram analysis,'' *Appl. Opt.* **32**, 3047–3052 (1993).
4. J. M. Huntley, ''Challenges in phase unwrapping,'' in *Trends in Optical Nondestructive Testing and Inspection*, P. K. Rastogi and D. Inaudi, Eds., pp. 37–44, Elsevier Science B.V., **City** (2000).
5. H. Tiziani, B. Franze, and P. Haible, ''Wavelength-shift speckle interferometry for absolute profilometry using a mode-hop free external cavity diode laser,'' *J. Mod. Opt.* **44**, 1485–1496 (1997).
6. M. Takeda and H. Yamamoto, ''Fourier-transform speckle profilometry: three-dimensional shape measurements of diffuse objects with large height steps and/or spatially isolated surfaces,'' *Appl. Opt.* **33**, 7829–7837 (1994).
7. C. Joenathan, B. Franze, P. Harble, and H. J. Tiziani, ''Speckle interferometry with temporal phase evaluation for measuring large-object deformation,'' *Appl. Opt.* **37**, 2608–2614 (1998).
8. C. Joenathan, B. Franze, P. Harble, and H. J. Tiziani, ''Large in-plane displacement measurement in dual-beam speckle interferometry using temporal phase measurement,'' *J. Mod. Opt.* **45**, 1975–1984 (1998).
9. C. Joenathan, B. Franze, P. Harble, and H. J. Tiziani, ''Novel temporal Fourier transform speckle pattern shearing interferometer,'' *Opt. Eng.* **37**(6), 1790–1795 (1998).
10. X. Li, G. Tao, and Y. Yang, ''Continual deformation analysis with scanning phase method and time sequence phase method in temporal speckle pattern interferometry,'' *Opt. Laser Technol.* **33**, 53–59 (2001).
11. M. Takeda, H. Ina, and S. Kobayashi, ''Fourier-transform method of fringe-pattern analysis for computer-based topography and interferometry,'' *J. Opt. Soc. Am.* **72**, 156–160 (1982).
12. I. Daubechies, *Ten Lectures on Wavelets*, Society for Industrial and Applied Mathematics, Philadelphia (1992).
13. G. H. Kaufmann and G. E. Galizzi, ''Speckle noise reduction in television holography fringes using wavelet thresholding,'' *Opt. Eng.* **35**(1), 9–14 (1996).
14. A. Federico and G. H. Kaufmann, ''Comparative study of wavelet thresholding methods for denoising electronics speckle pattern interferometry fringes,'' *Opt. Eng.* **40**(11), 2598–2604 (2001).
15. C. Shakher, R. Kumar, S. K. Singh, and S. A. Kazmi, ''Application of wavelet filtering for vibration analysis using digital speckle pattern interferometry,'' *Opt. Eng.* **41**(1), 176–180 (2002).
16. L. R. Watkins, S. M. Tan, and T. H. Barnes, ''Determination of interferometer phase distributions by use of wavelets,'' *Opt. Lett.* **24**, 905–907 (1999).
17. M. Afifi, A. Fassi-Fihri, M. Marjane, K. Nassim, M. Sidki, and S. Rachafi, ''Paul wavelet-based algorithm for optical phase distribution evaluation,'' *Opt. Commun.* **211**, 47–51 (2002).
18. J. Fang, C. Y. Xiong, and Z. L. Yang, ''Digital transform processing of carrier fringe patterns from speckle-shearing interferometry,'' *J. Mod. Opt.* **48**(3), 507–520 (2001).
19. X. Colonna de Lega, ''Continuous deformation measurement using dynamic phase-shifting and wavelet transform,'' in *Applied Optics and Optoelectronics 1996*, K. T. V. Grattan, Ed., pp. 261–267, Institute of Physics Publishing, Bristol (1996).
20. X. Colonna de Lega, ''Processing of non-stationary interference patterns: adapted phase shifting algorithms and wavelet analysis. Application to dynamic deformation measurements by holographic and speckle interferometry,'' Thesis 1666, Swiss Federal Institute of Technology Lausanne (1997).
21. M. Cherbuliez, P. Jacquot, and X. Colonna de Lega, ''Wavelet processing of interferometric signal and fringe patterns,'' *Proc. SPIE* **3813**, 692–702 (1999).
22. M. Cherbuliez and P. Jacquot, ''Phase computation through wavelet analysis: yesterday and nowadays,'' in *Fringe 2001*, W. Osten and W. Juptner, Eds., pp. 154–162, Elsevier, Paris (2001).
23. M. Cherbuliez, ''Wavelet analysis of interference patterns and signals: development of fast and efficient processing techniques,'' Thesis

Downloaded from SPIE Digital Library on 25 Aug 2010 to 155.69.4.4. Terms of Use: http://spiedl.org/terms

2377, Swiss Federal Institute of Technology Lausanne (2001).
24. A. Federico and G. H. Kaufmann, ''Evaluation of the continuous wavelet transform method for the phase measurement of electronic speckle pattern interferometry fringes,'' *Opt. Eng.* **41**, 3209–3216 (2002).
25. W. H. Press, S. A. Teukolsky, W. T. Vetterling, and B. P. Flannery, *Numerical Recipes in FORTRAN*, 2nd ed., Chap. 13, Cambridge University Press, Cambridge (1992).
26. S. Mallat, *A Wavelet Tour of Signal Processing*, Academic Press (1998).
27. N. Delprat, B. Escudie, P. Guillemain, R. Kronland-Martinet, P. Tchamitchian, and B. Torresani, ''Asymptotic wavelet and Gabor analysis: extraction of instantaneous frequencies,'' *IEEE Trans. Inf. Theory* **38**(2), 644–664 (1992).

Biographies and photographs of the authors not available.

Downloaded from SPIE Digital Library on 25 Aug 2010 to 155.69.4.4. Terms of Use: http://spiedl.org/terms